Impact of Geometric Parameters of Capillary Design on Quality of Gold Ball Bonding

Su, Jerry Chih-Tsong*, Yu, Cheng-Hsiang
Department of Mechanical and Automation Engineering
National Kaohsiung First University of Science and Technology
Kaohsiung 811, Taiwan, R.O.C.
Ph: 886-7-6011548; Fax: 886-7-6011548
Email: jerrysu@ccms.nkfust.edu.tw
*-Corresponding author

Abstract

0.13μm or smaller critical dimension of integrated circuits has driven the bonding pad pitch down to 50μm or even smaller. It has also had quite an impact on the adhesive force between the bonding pad and the gold ball. This study focuses on the correlation between the capillary geometric parameters (i.e. tip diameter, chamfer diameter, inner chamfer angle, and cone angle) and the bonding quality (i.e. ball size, ball thickness, ball shear force, specific ball shear force, and capillary vibration). An experimental design is utilized and the response is analyzed statistically. The results show that as the tip diameter and ball size increase, the ball thickness decreases, and the ball shear force increases first and then decreases afterward. As the cone angle decreases, the ball size increases, the ball thickness decreases, and the ball shear force increases. Therefore, both tip diameter and cone angle are significant factors that affect the bond quality. The empirical model, i.e. the correlation between the capillary geometric parameters and the bonding quality is also derived, and is quite useful in predicting the bonding pad size or bonding pad pitch required during process development. The predicted values and the experimental results are shown to have good agreement.

Key words

Semiconductor device packaging, Capillary, Gold ball bond, Response surface methodology.

1. INTRODUCTION

The smaller the critical dimension of a die the more challenges the bonding pad size or bonding pad pitch encounters. It is not only because the capability and stability of the machines become more difficult, but also because the design of the capillary, gold wire, lead frame and substrate of a die packaging face more limitations. The reliability of an integrated circuit is greatly dependent on the bonding quality of a die. The bonding quality is made up of the ball size, ball thickness, ball shear force, specific ball shear force, and capillary vibration. The bonding process is accomplished by the thermo-ultrasonic system [1, 2]. The normal rated static pressure is exerted on the capillary, and the vibration energy generates a fast relative motion on the contact surface of the shear force, and concluded that the optimal ratio is 81%. With respect to the formation of the loop, Barez [10] and gold ball and the bonding pad, between which a metallic atomic bond is formed [3, 4]. The entire gold wire bonding process can be divided into: 1. formation of gold ball before bonding, 2. ball bond, 3. formation of loop, and 4. stitch bond.

Hu [5] indicated that the bonding quality becomes worse if the ball is in the shape of a golf ball before the gold wire is bonded. Lee [6], Pantaleon [7], and Kinnaird [8] concluded that the ball shear force of the ball bond depends critically on the ball size and ball thickness. In order to have the best bonding quality for the ball bond, it is necessary to control the ball size and ball thickness. Aguila [9] studied the correlation of the ratio of the actual welding area of the ball bond to the ball size and the ball Groover [11] studied the optimization method for controlling the height of the loop and the important factors

that affect the stability of the looping. Pecht [12] assured the quality of bonding and shortend the testing time by using the tension test technology.

Chen [13] studied the optimal parameters for the gold ball formation. Shu [14] and Su [15] studied the optimization of the operating parameters such as the machine bond, power, bond force, bond time and operating temperature. Or [1] proposed that the instant monitoring method for the wire bonding process quality can allow users to immediately observe the bonding quality. Liang's [16] bonding reliability measurement method helps to analyze the bonding quality. The study by Saboui [17] showed that after the bonding pad pitch is reduced, the selection of the capillary is very important, and the design of geometric parameters is one of the important factors for obtaining the best quality of gold ball bonding.

From the above literature, it is known that the geometric parameters of the capillary greatly affect the bonding quality, but few studies investigate their relationship. This article focuses on the design of capillary geometric parameters and studies the resulting impact on the ball bond quality. This article also studies capillary vibration (i.e. the relation between the capillary parameter and displacement of ultrasonic vibration), which has rarely been reported before.

2. EXPERIMENTAL PROCEDURE

There are many factors affecting the bonding quality of the gold ball. They are complicated and not easily analyzed by analytical methods; therefore the design of experiment (DOE) is employed in this study [18]. This study explores the relations between the geometric parameters of the capillary and the bonding quality of the ball bond. The experimental procedures of this research follow the sequences: 1. Fish-bone diagram analysis 2. Design of gold ball size 3. Locate machine's electrical flame off parameters 4. Locate machine's bonding parameters 5. Define capillary parameters 6. Design of experiment 7. Capillary vibration experiment 8. Data collection 9. Regression analysis 10. Model.

2.1 Ball Shape Design Before/After Bonding

From the fish-bone diagram analysis, it is known that the major capillary geometric parameters, which affect bonding quality, include four factors, i.e. tip diameter (D_T), chamfer diameter (D_c), inner chamfer angle (ϕ_c) and cone angle (ϕ_T). The detailed geometric parameter definitions of the capillary are shown in Fig. 1.

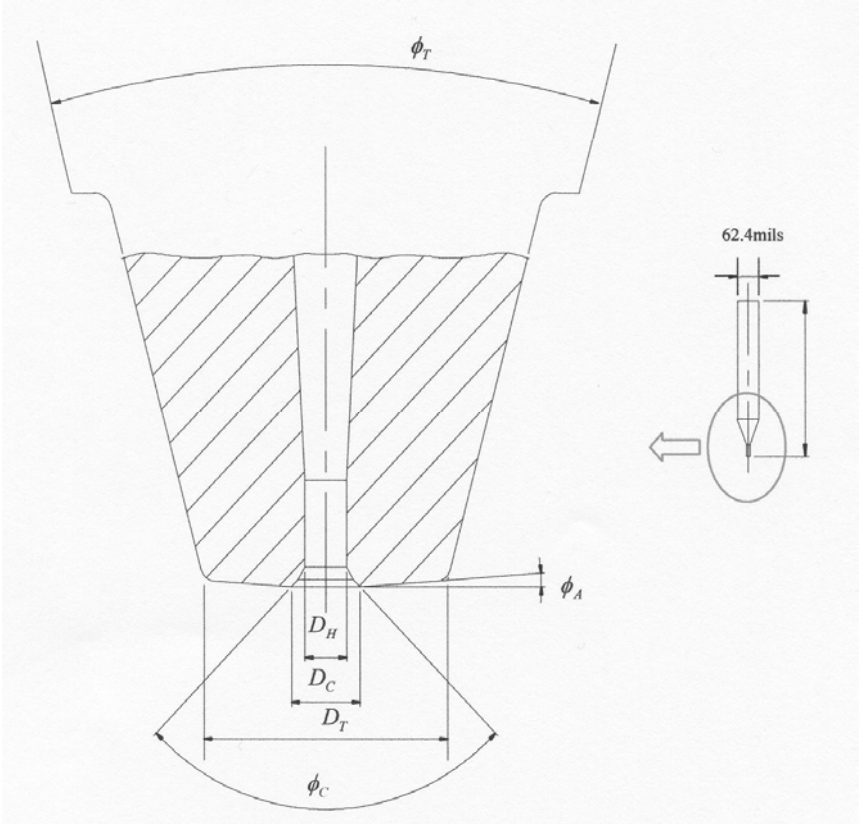

Fig. 1. Illustrations of capillary geometry parameters

Firstly, the essential guideline for selecting diameter *d* of the gold ball, shown in Fig. 2,

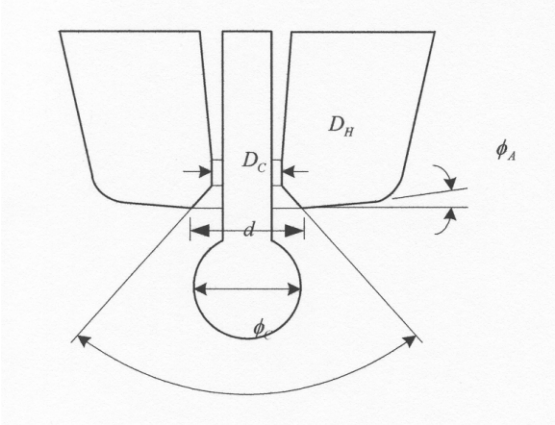

Fig.2. Free air ball

before bonding and the ball thickness h_b, shown in Fig. 3,

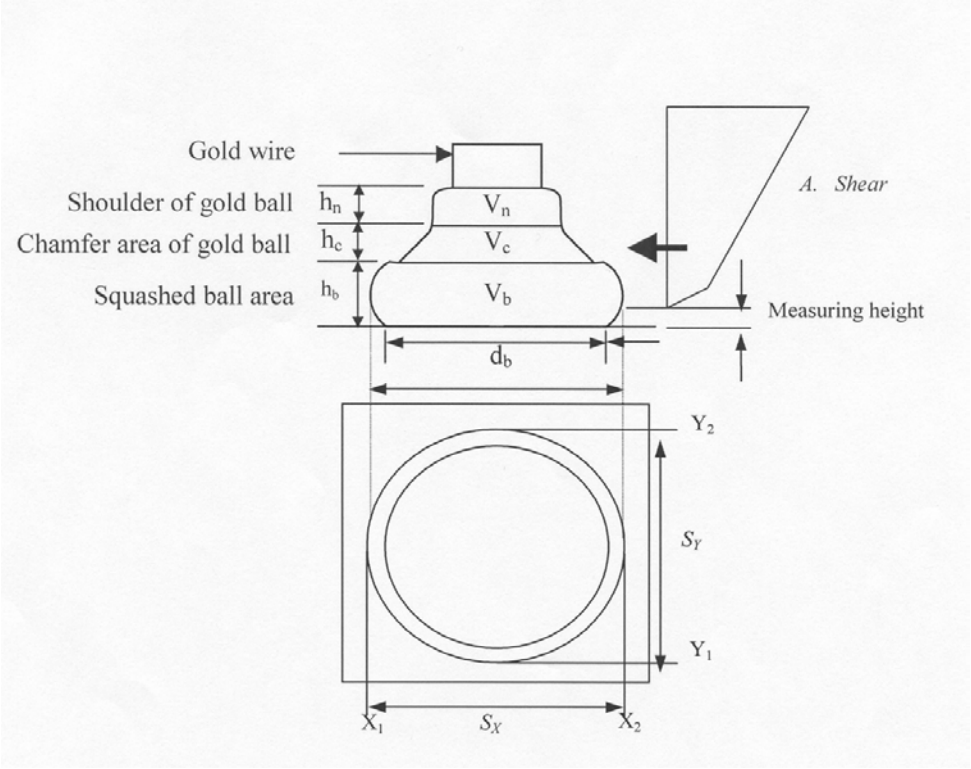

Fig.3. Illustrations of the ball size and shear tool

after bonding is that the total volume should remain unchanged, and the expressions are given below [17].

$$V_t = V_n + V_c + V_b \quad (1)$$

$$V_t = \frac{\pi}{6} \times d^3 \quad (2)$$

$$V_b = \frac{\pi}{4} \times d_b^{\,2} \times h_b - \frac{\pi}{24} \times (d_b^{\,2} + d_b \times D_c + D_c^{\,2}) \times (d_b - D_c) \times \tan\phi_A \quad (3)$$

$$V_c = \frac{\pi}{12} \times (D_H^{\,2} + D_H \times D_c + D_c^{\,2}) \times \tan\left(\frac{180° - \phi_c}{2}\right) \times \left(\frac{D_c - D_H}{2}\right) \quad (4)$$

$$V_n = \frac{\pi}{4} \times D_H^{\,2} \times h_n \quad (5)$$

V_t : Total volume of gold ball.

V_b : Volume of the squashed ball area after gold ball bonding.

V_c : Volume of the chamfer area after gold ball bonding.

V_n : Volume of the shoulder after gold ball bonding.

h_b : Height of the squashed ball area after gold ball bonding.

h_n : Height of the shoulder of the gold ball after gold ball bonding.

h_c : Height of the chamfer area after gold ball bonding.

D_H : Hole diameter of capillary.

D_c : Chamfer diameter of capillary.

ϕ_A : Face angle of capillary.

ϕ_c : Inner chamfer angle of capillary.

2.2 Bonding and Electrical Flame Off Parameters of Experiment Machines

Before performing the design of experiment of capillary geometric parameters, the electrical flame off parameters and the optimized process parameters of the machine for ball bonding should be determined.

This study takes a 90μm bonding pad pitch as an example, which defines the standard ball thickness (h_b) after bonding as 0.6mil, the diameter of the squashed ball is equal to 2.8mil, and the diameter of the gold ball before bonding follows the design as described in Section 2.1 to control its value within the range of 2~2.293mil. Because the internal diameter (D_H) of the capillary is 1.5mil, the diameter of the gold ball before bonding should be selected as 2.2mil to avoid abnormal bonding due to the manufacturing tolerance of the capillary, gold wire and the stability of the electrical

flame off. Thus, the electrical flames off parameters are determined.

The Taguchi method is used to determine the optimized process parameters of the ball bonding for the machine. There are three bonding parameters: bond time, bond power, and bond force. Experiments designed by orthogonal array $L_4 2^3$ of the Taguchi method were performed and the measurements were taken and analyzed by variance analysis to obtain the optimized parameters, that is, bond time: 20ms, bond power: 90mw, and bond force: 30g. These process parameters were also verified and used through the design of experiment of capillary geometry.

2.3 Design of Experiment of Capillary Geometric Parameters

Based on the test samples of 90μm bonding pad pitch, the ranges of the geometric parameters of the capillary in the experiments are given below:

Factor A : Tip diameter (D_T): Parameter ranges 4~6 mil, and mean value is 5 mil.

Factor B : Chamfer Diameter (D_C): Parameter ranges 1.9~2.5 mil, and mean value is 2.2 mil.

Factor C : Inner Chamfer Angle (ϕ_C): Parameter ranges 90°~120°, and mean value is 105°.

Factor D : Cone Angle (ϕ_T): Parameter ranges 20°~30°, and mean value is 25°.

The scheme of central composite design (CCD) was employed to obtain 27 experiment runs shown in Table 1. According to the aforementioned experiment sequence, the bonding samples of 90μm ball grid array (BGA), the wire diameter of 1.28mil, and the bonding machine were used. After performing the experiment, thirty-two points were randomly selected from the bonding sample for each experiment, and the ball size, ball thickness, and ball shear force were measured. The method of measuring of the observed values in this study is described in Section 2.4.

Table 1. Design of experiment for capillary geometric parameter and measurements.

Run No.	D_T (mil)	D_C (mil)	ϕ_C (degree)	ϕ_T (degree)	S_x (μm)	S_y (μm)	h_b (μm)	BSF(F_s) (gm)	Specific BSF (f_s) (gm/mil^2)
1	4	1.9	90	20	69.57	69.21	17.69	27.18	4.64
2	6	1.9	90	20	77.23	74.85	11.85	26.13	3.71
3	4	2.5	90	20	69.23	67.52	14.36	32.16	5.65
4	6	2.5	90	20	76.86	76.28	9.62	28.47	3.99
5	4	1.9	120	20	70.18	67.91	18.56	30.30	5.22
6	6	1.9	120	20	78.75	74.43	13.27	26.47	3.71
7	4	2.5	120	20	69.67	68.79	16.03	26.84	4.60
8	6	2.5	120	20	76.93	75.65	10.86	27.98	3.95
9	4	1.9	90	30	66.83	64.94	20.54	21.65	4.09
10	6	1.9	90	30	78.22	76.41	11.42	26.38	3.63
11	4	2.5	90	30	66.31	66.71	15.87	25.97	4.83
12	6	2.5	90	30	74.79	74.59	11.88	31.88	4.69
13	4	1.9	120	30	68.58	66.52	19.52	25.78	4.64

14	6	1.9	120	30	78.83	73.99	12.95	26.00	3.66
15	4	2.5	120	30	67.60	65.74	16.41	27.50	5.08
16	6	2.5	120	30	75.01	72.97	11.32	29.06	4.36
17	3	2.2	105	25	65.41	64.58	16.73	14.74	2.87
18	7	2.2	105	25	76.53	75.55	10.19	27.76	3.96
19	5	1.6	105	25	73.93	70.70	14.83	29.53	4.65
20	5	2.8	105	25	69.95	70.35	12.42	34.42	5.74
21	5	2.2	75	25	72.45	72.40	13.51	33.99	5.32
22	5	2.2	135	25	69.98	67.54	12.69	29.45	5.13
23	5	2.2	105	15	78.13	76.63	9.77	26.61	3.67
24	5	2.2	105	35	68.37	66.52	16.25	35.21	6.35
25	5	2.2	105	25	71.51	71.00	14.67	33.15	5.37
26	5	2.2	105	25	71.59	71.05	13.84	30.45	4.93
27	5	2.2	105	25	73.92	72.81	13.46	29.60	4.51

2.4 Measuring the Experiment Sample

Besides the ball size, ball thickness, and ball shear force, the bonding quality of gold ball bond also includes the specific ball shear force and capillary vibration. The measurements taken and measuring methods are described below: (Steps a ~ e):

a. Ball size measurement defined in Fig. 3 [14, 19]:
Ball diameter in X- direction (S_X) = measured value from X_1 to X_2
Ball diameter in Y- direction (S_Y) = measured value from Y_1 to Y_2

b. Ball thickness measurement: h_b in Fig. 3 is the actual ball thickness.

c. Ball shear force (F_S): The shear force is measured by a shear tool at a height of 3~5μm from the bonding pad in Fig. 4.

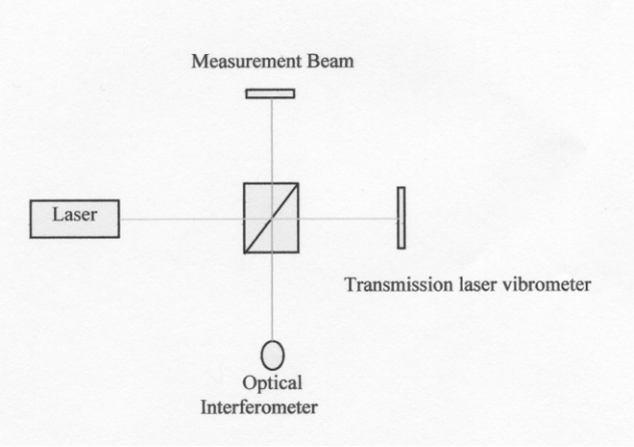

Fig.4. Illustrative diagram of capillary vibration measurement

d. Specific ball shear force (f_S): The measured values of the ball diameter in X and Y axes are larger than the actual bonded area and almost show a parabolic relation, which can be represented by

$$f_S = 4 * F_S \Big/ [\pi * (S_X * S_Y)]$$ as in [16].

e. Capillary vibration S_V : A transmission laser vibrometer is used for the measurement: a light beam is emitted by the laser source, and such beam is mixed by the optical

interferometer, and the photo detector measures the strength of the mixed light and the phase difference. The magnitude of capillary vibration is obtained from the variation of the phases [2] as shown in Fig. 4. The relationship between the capillary and the characteristic of vibration is described in Section 2.5.

2.5 Design of Experiment for Capillary Vibration Measurement

According to field experience, the energy of ultrasonic vibration relates to the bonding quality, and the physical meaning of the ultrasonic wave on bonding is the magnitude of vibration [20,21]. To understand the relation between the capillary geometric parameters and the capillary vibration, the experiment of the capillary vibration is designed.

From capillary manufacturing experience, the capillary vibration has no relation with the chamfer diameter (D_C) and inner chamfer angle (ϕ_C). To simplify the capillary experiment, two groups of capillaries with a total number of four experiments were performed and measured by transmission laser vibrometer to compare the differences of capillary vibrations [22]. The trend from the observations is used to verify whether or not there is an effect of the chamfer diameter (D_C) and inner chamfer angle (ϕ_C) on capillary vibration.

2.5.1 Group 1. Measurement of Capillary Vibration for Capillaries A and B

Two capillaries A and B with different chamfer diameters (CD) are used to measure the capillary vibration, and the capillary diameters are shown below:

Capillary A: $D_T = 4\text{mil}$, $D_C = 1.9\text{mil}$, $\phi_C = 90°$, $\phi_T = 30°$

Capillary B: $D_T = 4\text{mil}$, $D_C = 2.5\text{mil}$, $\phi_C = 90°$, $\phi_T = 30°$

Firstly, measure the magnitude of the vibration along the axis of the capillary, i.e. from the root to the tip of the capillary, and normalize the measured values. Represent the measured data in the distribution graph as shown in Fig. 5, where the X-axis is the position of the capillary vibration and the Y-axis is the normalized vibration displacement. From Fig. 5, it shows that there is no significant difference in capillary vibration between capillary A and B. Since the chamfer diameter (D_C) has no effect on the capillary vibration, it will be ignored in the capillary experiment.

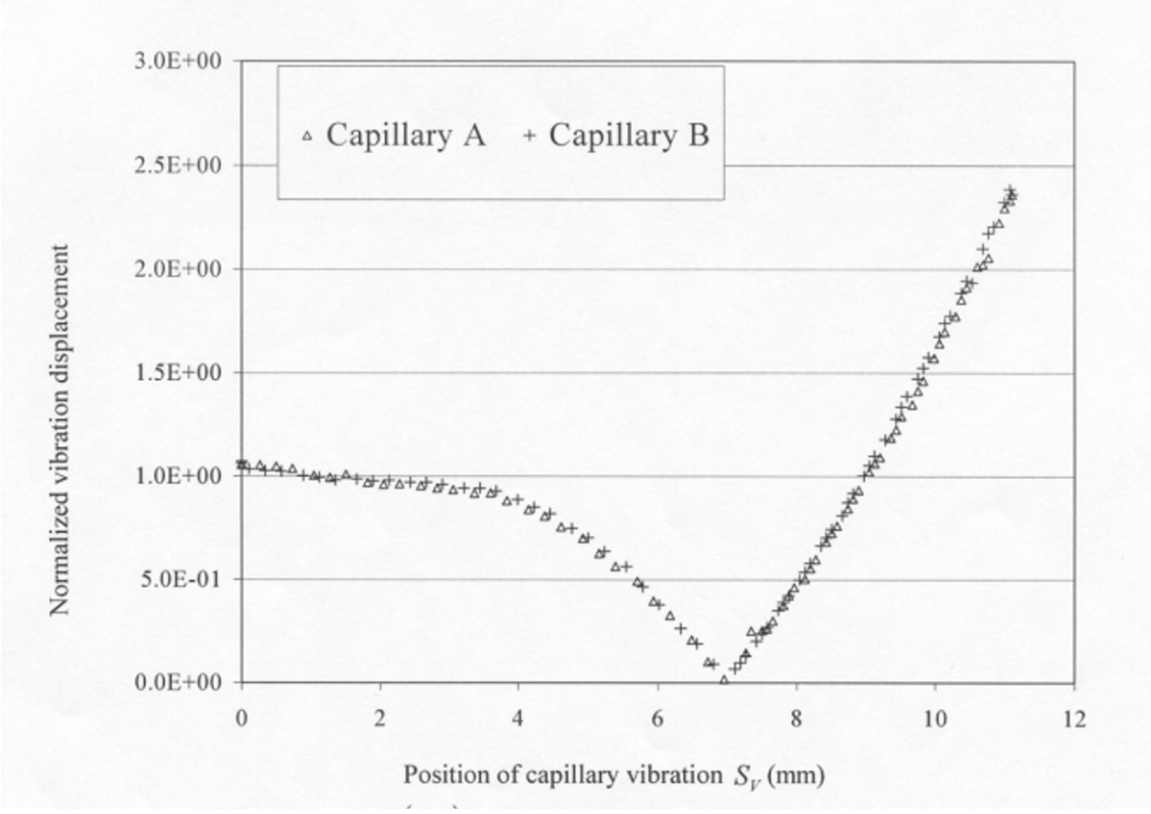

Fig. 5. Normalized vibration displacement with various Chamfer Diameter (D_C)

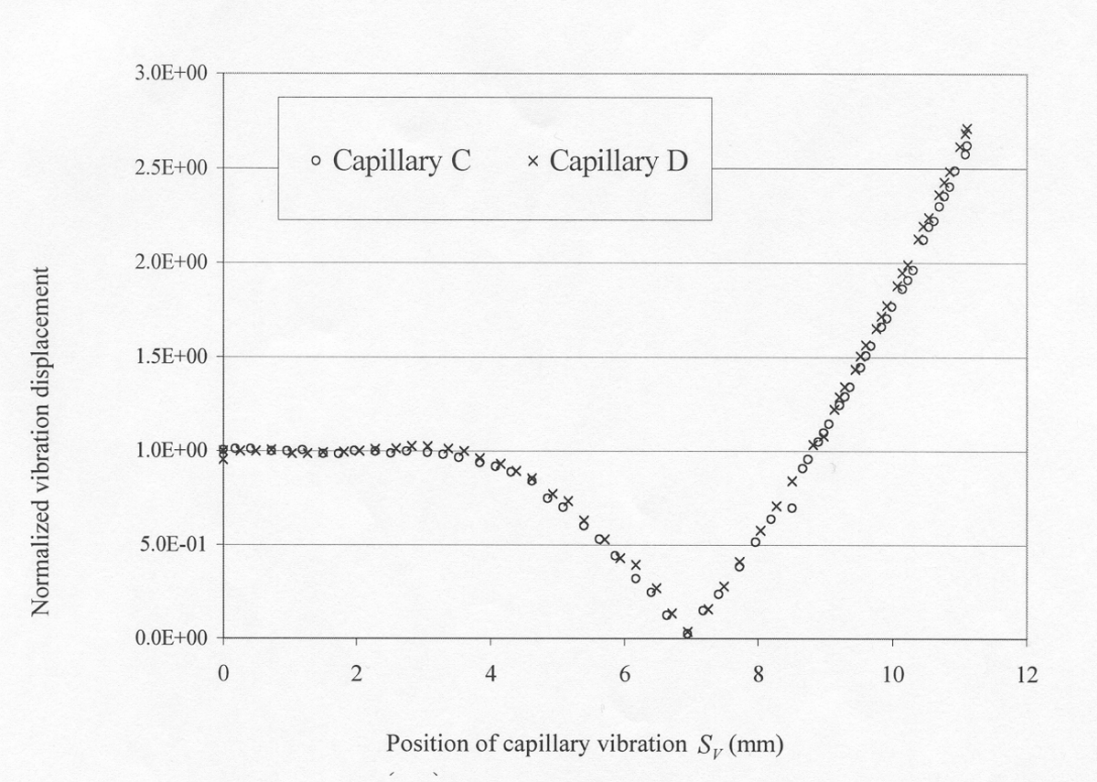

Fig. 6. Normalized vibration displacement with various Inner Chamfer Angle (ϕ_C)

2.5.2 Group 2. Measurement of Capillary Vibration for Capillaries C and D

Similarly, two capillaries C and D with different inner chamfer angles (ϕ_C) were designed to perform the experiment and the capillary vibration is shown in Fig. 6. It should be noted that the inner chamfer angle (ϕ_C) has no effect on the capillary vibration; therefore the inner chamfer angle (ϕ_C) will also be ignored in the capillary experiment.

Capillary C: D_T = 4mil, D_C = 2.5mil, ϕ_C = 90°, ϕ_T = 20°

Capillary D: D_T = 4mil, D_C = 2.5mil, ϕ_C = 120°, ϕ_T = 20°

3. RESULTS AND DISCUSSION

This study explores the correlations between the capillary geometry parameters and the bonding quality of the gold ball. The measured data of the experiments includes six items: 1. Ball diameter in the X -axis, 2. Ball diameter in the Y-axis, 3. Ball thickness, 4. Ball shear force, 5. Specific ball shear force, and, 6. Capillary vibration. The measured data is analyzed by the procedures: 1. Model forming, 2. Statistical testing, 3. Model refining, and 4. Regression analysis. The preliminary model is first examined by the F test, and the level of confidence (i.e. α value) is set to 0.05. The analysis of variance (ANOVA) is performed to select the major effects and the interactions of the parameters. The refined model is determined after eliminating the unimportant factors and testing the fitness of the preliminary model. Finally, the regression equation is selected by residual analysis and verified by the normality check, and the 3-D response surface and the contour plots are constructed.

The regression equations of the six measured responses are shown in (6)-(11), respectively, after the regression analyses.

Ball diameter in X-axis :

$$S_X = 66.17 + 3.79 \times D_T - 2.74 \times D_C - 0.26 \times \phi_T \quad (6)$$

Ball diameter in Y-axis :

$$S_Y = 60.37 + 3.49 \times D_T - 0.27 \times \phi_T \quad (7)$$

Ball thickness :

$$h_b = 29.49 - 2.45 \times D_T - 3.37 \times D_C + 0.17 \times \phi_T \quad (8)$$

Ball shear force :

$$F_S = -218.39 + 77 \times D_T + 12.678 \times \phi_T + 4.1333 \times D_C + 0.248 D_T \times \phi_T - 14.02 \times {D_T}^2 - 0.57 \times {\phi_T}^2 + 0.76 \times {D_T}^3 + 0.0076 \times {\phi_T}^3 \quad (9)$$

Specific ball shear force :

$$f_S = -52.953 + 21.62 \times D_T + 0.8333 \times D_C + 2.25 \times \phi_T - 4.03 \times {D_T}^2 - 0.09 \times {\phi_T}^2 + 0.24 \times {D_T}^3 + 0.0012 \times {\phi_T}^3 \quad (10)$$

Capillary vibration :

$$S_V = 1.08 - 0.00233 \times D_T - 0.062 \times \phi_T + 0.00107 \times {\phi_T}^2 \quad (11)$$

Where

$4 \text{ mil} \leq D_T \leq 6 \text{ mil}$

$1.9 \text{ mil} \leq D_C \leq 2.5 \text{ mil}$

$90^o \leq \phi_C \leq 120^o$

$20^o \leq \phi_T \leq 30^o$

From (6)-(8), it is clear that there are no interactions between parameters. The residual value R^2 of (6)-(8), i.e. the regression equations of the ball diameter in X- and Y-axis, and the ball thickness, are 87.34%, 85.49%, and 82.83%, respectively. (9)-(11), which include the interactions of the quadratic and cubic terms, show the regression equations of the ball shear force, the specific ball shear force, and the capillary vibration. Equations (9)-(11) have residual value R^2 of 83.42%, 80.82%, and 84.66%, respectively.

In (11), the tip diameter is insignificant according to variance analysis and should be eliminated. The regression equation after the factor of tip diameter is deleted and simplified:

$$S_V = 1.06 - 0.062 \times \phi_T + 0.00107 \times {\phi_T}^2 \quad (12)$$

Because the residual value R^2 of (12) is 84.51%, which is not much different from 84.66% obtained from (11), it is decided to keep the linear term of tip diameter in (11) to facilitate the generation of the 3-D response plots

3.1 Discussion

Figs. 7~12, which are obtained by equating the mean values D_C =2.2mil and ϕ_C =105° in (6)-(11), show the six 3-D response plots of the observed values of the bonding quality in the capillary experiment. The detailed discussions are given below:

3.1.1 Ball diameter in X-axis S_X

From Fig. 7, the ball size increases as the tip diameter increases or as the cone angle decreases. In the range of design parameter, the maximum and minimum ball sizes are 77.6μm and 67.3μm repectively, the difference is 10.3μm, and the mean value is 72.45μm, which is larger than the target value 71.12μm (2.8mil). Obviously, it has worse control on the ball size in the X direction. It can be seen that the impact of the tip diameter is more significant than that of the cone angle. In other words, the tip diameter is the primary factor affecting the ball diameter in the X-axis S_X, and the cone angle ϕ_T is the secondary factor.

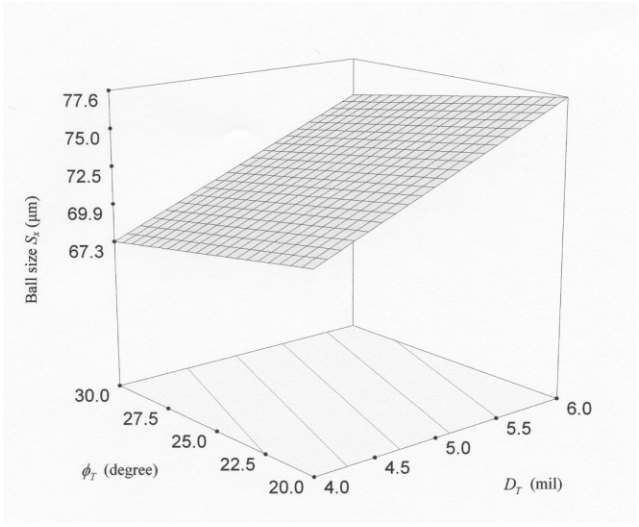

Fig. 7. 3-D response plot of ball diameter S_x in X-axis

3.1.2 Ball diameter in Y-axis S_Y

From Fig. 8, the ball size linearly increases as the tip diameter increases or as the cone angle decreases. In Fig. 8, the maximum ball size is 75.8μm, the minimum ball size is 66.1μm, the difference is 9.7μm, the mean value is 70.95μm, which is very close to the target value of 71.12μm (2.8mil). Obviously, the control ability of ball size in the Y-axis is better than that in the X-axis. In addition, it also can be seen that the effect of tip diameter is more significant than that of cone angle; it shows that the tip diameter is also a primary factor affecting the ball diameter in the Y-axis, and the cone angle is the secondary factor.

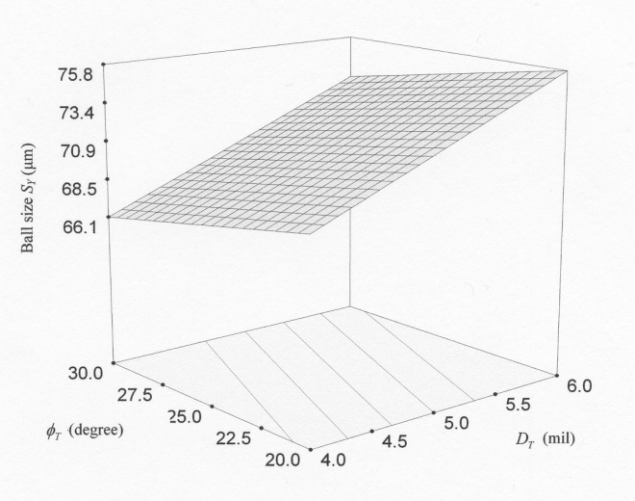

Fig. 8. 3-D response plot of ball diameter S_Y in Y-axis

3.1.3 Ball thickness h_b

The ball thickness in Fig. 9 decreases as the tip diameter increases or as the cone angle decreases. Comparing Fig. 9 with Figs. 7 and 8, it can be seen that the ball diameter in the X and Y-axis increases as the tip diameter increases, but the ball thickness decreases as the tip diameter increases. It shows that the tip diameter is the primary factor that affects the ball thickness, and the cone angle and the chamfer diameter are secondary factors.

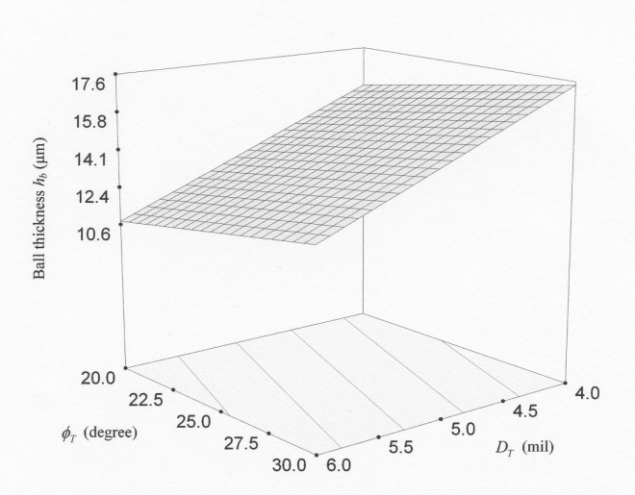

Fig. 9. 3-D response plot of ball thickness h_b

3.1.4 Ball shear force F_S

From Fig. 10, when the tip diameter is 4mil, the ball shear force decreases significantly as the cone angle increases, but if the tip diameter is equal to 6mil, then even the cone angle increases from 20° to 30°; the ball shear force remains unchanged. If the tip diameter is equal to 4.8mil, the ball shear force reaches the maximum. In other words, when the diameter of the gold ball is 2.2mil before bonding, free air ball (FAB), and the bonding parameters of the machine are: Bond Time=20ms, Bond Power=90mw, Bond Force=30g and the tip diameter of the capillary is equal to 4.8mil, the best ball shear force is obtained. It can be seen that the tip diameter is the primary factor that affects the ball shear force.

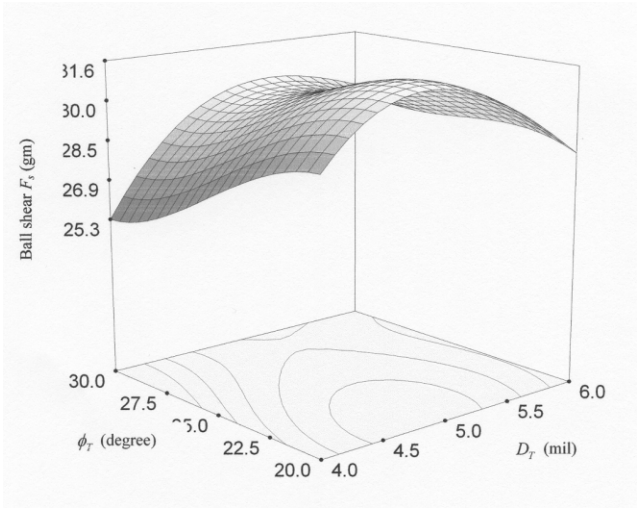

Fig.10. 3-D response plot of ball shear force F_S

3.1.5 Specific ball shear force f_S

From Fig. 11, one can see that the specific ball shear force decreases as the tip diameter increases. The effect of cone angle is not as significant as the tip diameter on the specific ball shear force. The maximum occurs when the tip diameter is in the neighborhood of 4.8mil. From the analysis of variance, the tip diameter is the primary factor that affects the specific ball shear force for both the linear and the quadratic terms have very significant effects.

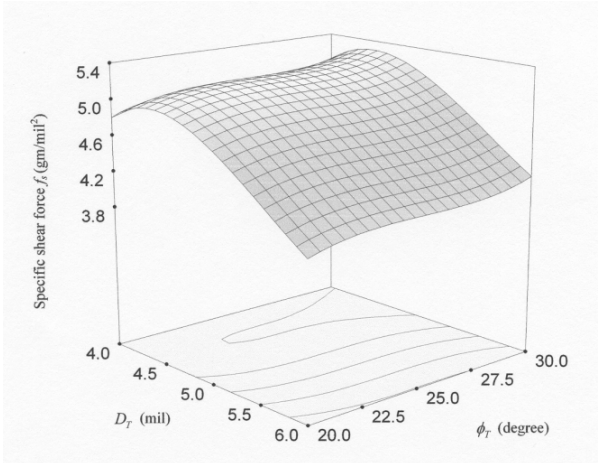

Fig.11. 3-D response plot of specific ball shear force f_s

3.1.6 Capillary vibration S_V

From Fig. 12, one can see that the capillary vibration rapidly increases from 0.16μm to 0.25μm as the cone angle decreases from 30° to 20°. The variation of tip diameter has no significant effect on the magnitude of vibration. Since the ball size in Figs. 7 and 8 increases as the cone angle decreases, therefore capillary vibration is related to ball size. From the analysis of variance, it can be seen that the cone angle is the primary factor that affects the capillary vibration, and the effect of tip diameter on the magnitude of vibration is not significant.

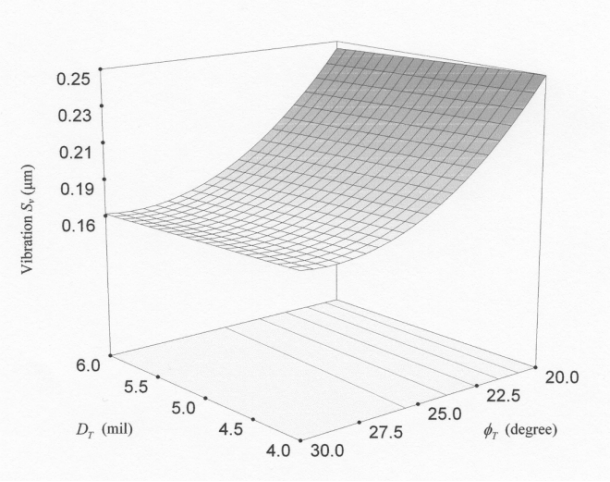

Fig. 12. 3-D response plot of capillary vibration S_v

3.2 Verification

To verify the regression model of the capillary geometry and the bonding quality, a newly designed capillary is selected with the following parameters:

hole diameter (D_H) = 1.5mil
chamfer diameter (D_C) = 2.0mil
inner chamfer angle (ϕ_C) = 90°
cone angle (ϕ_T) = 30°
tip diameter (D_T) = 4.0mil
face angle (ϕ_A) = 11°

The experiment of verification firstly estimates the bonding quality according to the regression models in the discussion in Section 4 and the specifications of the newly designed capillary mentioned above. Then, the 90μm BGA (Ball grid array) samples and the same type of wire bonder, which used consistent process parameters: the bond time: 20ms, bond power: 90mw, and bond force: 30g, were selected to run the experiment. The target value of the diameter of free air ball (FAB) before bonding is still 2.2mil (56μm). Thirty-two samples were measured and analyzed to compare with the predicted values that were obtained from the regression model. The bonding quality, estimated by the regression model and calculated from the measured data, respectively, is shown in Table 2.

Table 2. Bonding quality calculated from regression model and measured data.

	From regression model			Measured data
Bonding quality	Target	Eq. No.	95% confidence interval	Average
Ball diameter in X	67.92μm	6	64.4~71.43μm	69.29μm
Ball diameter in Y	66.12μm	7	62.74~69.49μm	68.77μm
Ball thickness	18.06μm	8	15.2~20.93μm	19.9μm
Ball shear force	24.6gm	9	20.23~28.97gm	28.76gm
Specific ball shear force	4.93gm/mil^2	10	4.08~5.78 gm/mil^2	4.95gm/mil^2
Capillary vibration	0.171μm	11	0.088~0.254μm	0.24μm

The free air ball used for verification was measured to have an average ball diameter of 56.94μm, which was 0.94μm larger than the target value of 56μm. Comparing the predicted values and the experimental values, it can be seen that the experimental values are all within the 95% confidence interval of the predicted values, although they are somewhat closer to the upper bounds. However, after compensating the 0.94μm difference between predicted and target ball diameter of free air ball, the experimental values should be not only within the 95% confidence interval of the predicted values, but also closer to the target values. In other words, the experiment verifies the regression models of the bonding quality and the capillary geometry. From this, one can conclude that the response plots and correlations, (6)-(12), which are obtained from the regression models, are quite useful in predicting the bonding quality and optimizing the capillary geometry.

4. CONCLUSION

This study employs the central composite design to obtain the regression models of the bonding quality and the capillary geometry. The following conclusions can be drawn:

(1) The primary factor affecting ball diameters in the X and Y-axis is the tip diameter, and the secondary factor is cone angle. The ball diameter in the X and Y-axis linearly increases as the tip diameter increases or the cone angle decreases.

(2) The primary factor affecting ball thickness is the tip diameter, and the secondary factors are cone angles and chamfer diameter. The ball thickness linearly decreases as the tip diameter increases or as the cone angle decreases.

(3) The primary factor affecting ball shear force is the tip diameter, and the secondary factors are cone angles and chamfer diameter. When the tip diameter is equal to 4 mil, the ball shear force decreases as the cone angle increases. But the ball shear force is not obviously changed when the tip diameter equals 6mil, no matter what the cone angle is. If the tip diameter is 4.8mil, then the ball shear force reaches the maximum.

(4) The primary factor affecting specific ball shear force is the tip diameter, and the secondary factor is the chamfer diameter. The specific ball shear force decreases as the tip diameter increases. When the tip diameter is equal to 4.8mil, then the specific ball shear force is the maximum. The result of the specific ball shear force is quite similar to that of the ball shear force.

(5) The primary factor affecting the capillary vibration is the cone angle, and the capillary vibration increases as the cone angle decreases.

(6) If the capillary geometry parameter falls in the domain of the design experiment, the bonding quality of the gold ball bonding can be predicted by the response plots and correlations, (6)-(12), obtained from the regression equations, which makes the selection of the bonding tool faster and more efficient.

When the bonding pad pitch or bonding pad open area is reduced, the capillary geometry parameter needs to be redesigned and the bonding quality also requires improvement. In this case, the regression models are useful in providing the capillary users in predicting capillary geometry parameters. Besides, the regression models also provide important results of simulation and data information to the capillary designers to optimize the bonding tools and bonding quality.

References

[1] S. W. Or, et al., "Ultrasonic wire bond quality monitoring using piezoelectric sensor," Sensor and Actuator A: physical, Vol. 65, pp. 69-75, Feb., 1998.

[2] S. W. Or, et al., "Dynamics of an ultrasonic transducer used for wire bonding," Ultrasonics, Vol. 45, No. 6, pp. 1453-1460, 1998.

[3] J. Tsujino, "Welding characteristics and temperature rise of high frequency and complex vibration ultrasonic wire bonding," Ultrasonics, Vol. 36, pp. 59-65, 1998.

[4] P. Schwaller, et al., "Surface and friction characterization by thermoelectric measurements during ultrasonic friction process," Ultrasonics, Vol. 38, pp. 212-214, March, 2000.

[5] S. J. Hu, R. K. S. Lim and G. Y. Sow, "Gold wire weakening in the thermosonic bonding of the first bond," IEEE Transactions on Packaging and Manufacturing Technology, Vol. 18, pp. 230-234, March, 1995.

[6] H. K. Lee and S. I. Yoo, "An automated method for inspection of IC bonds," ICCIMA '99, 3rd Conference, pp. 176-180, 1999.

[7] R. Pantaleon, et al., "Rationalization of gold ball bond shear strengths," 44th Electronic Components and Technology Conference Proceedings, pp. 733-740, 1994.

[8] C. D. Kinnaird, and A. Khotanzad, "Adaptive fuzzy process control of integrated circuit wire bonding," IEEE Transactions on Electronics Packaging Manufacturing, Vol. 22, pp. 233-243, July, 1999.

[9] T. Aguila, et al., "Ball bond characterization: An intensive analysis on ball size and shear test results and applicability to existing standards," 1st Electronic Packaging Technology Conference, pp. 46-51, 1997.

[10] F. Barez, "Optimization of wire loop height for a cavity down plastic pin grid array package," ASME Transactions, Vol. 120, pp. 194-200, June, 1998.

[11] R. Groover, W. K. Shu and S. S. Lee, "Wire bond loop profile development for fine pitch-long wire assembly," IEEE Transactions on Semiconductor Manufacturing, Vol. 7, pp. 393-399, August, 1994.

[12] M. Pecht, D. Barker and P. Lall, "Development of an alternative wire bond test technique," IEEE Transactions on Packaging and Manufacturing Technology, Vol. 17, pp. 610-615, December, 1997.

[13] J.-L. Chen and Y.-C. Lin, "New approach in free air ball formation process parameters analysis," IEEE Transactions on Electronics Packaging Manufacturing, Vol. 23, pp. 116-122, April, 2000.

[14] W. K. Shu, "Fine pitch gold bonding optimization," Electronics Manufacturing Technology Symposium, 15th IEEE/CHMT, pp. 37-44, 1993.

[15] C.-T. Su and T.-L. Chiang, "Optimal design for a ball grid array wire bonding process using a neuro-genetic approach," IEEE Transactions on Electronics Packaging Manufacturing, Vol. 21, pp. 13-18, January, 2002.

[16] Z. N. Liang, F. G. Kuper and M. S. Chen, "A concept to relate wire bonding parameters to bondability and ball bond reliability," Microelectronics Reliability, Vol. 38, pp. 1287-1291, June, 1998.

[17] A. Saboui, "Wire bonding limitations for high density fine pitch plastic packages," Electronics Manufacturing Technology Symposium, 11th IEEE/CHMT, pp. 75-79, 1991.

[18] D. C. Montgomery, Design and Analysis of Experiments, Third Edition, John Wiley & Sons Inc., 1991.

[19] B. Shu, "Fine pitch wire bonding development using a new multipurpose multi-pad pitch test die," 41st Electronic Component and Technology Conference Proceedings, pp. 511-518, May, 1991.

[20] C. M. Hu, et al., "The vibration characteristics of capillary in wire bonder," Electronics Packaging Technology Conference, pp. 202-205, 1998.

[21] J. Schwizer, et al., "Thermosonic ball bonding: Friction model based on integrated microsensor measurements," Electronics Manufacturing Technology Symposium, 24th IEEE/CPMT, pp. 108-114, 1999.

[22] Y. Tamura, et al., "Analysis and application of vibration behavior for wire bonding capillary by transmission laser vibrometer," Electronics Manufacturing Technology Symposium, 23rd IEEE/CPMT, pp. 72-75, 1998.